

A Low-Cost, User-Friendly Rheo-Optical Compression Assay to Measure Mechanical Properties of Cell Spheroids in Standard Cell Culture Plates

Rosalia Ferraro, Sergio Caserta,* and Stefano Guido

The mechanical characterization of cell spheroids, one of the most widely used 3D biology models *in vitro*, is a hotspot of current research on the role played by the mechanical response of cells and tissues. The techniques proposed so far in the literature, while providing important scientific insights, require specialized equipment and technical skills that are not usually available in cell biology facilities. Here, an innovative rheo-optical compression assay is presented: it is based on microscopy glass coverslips as the load is applied to cell spheroids in standard cell culture plates and on image acquisition with an optical microscope or even a smartphone equipped with adequate magnification lenses. Mechanical properties can be simply obtained by correlating the applied load to the deformation of cell spheroids measured by image analysis. The low-cost, user-friendly features of the proposed technique can boost mechanobiology research making it easily affordable to any biomedical lab equipped with cell culture facilities.

1. Introduction

Cell spheroids, defined as self-assembled 3D cell aggregates *in vitro*,^[1] are a widespread model of tissue microenvironment used to recapitulate cell-cell and cell-extracellular matrix (ECM) interactions in several physio-pathological processes.^[2,3] Due to their structural and functional similarities with *in vivo* tumors,^[4–6] spheroids have emerged as a valuable tool in cancer research. In fact, being characterized by the presence of chemical gradients (i.e., oxygen, nutrients, and catabolites), cellular spheroids mimic

the heterogeneous structure of tumors and generally consist of three regions^[7]: an outer shell with actively proliferating cells, a middle region with quiescent cells, and a nutrient deprived zone (necrotic core)^[8] in the center, due to lack of nutrients and accumulation of waste induced by diffusion limitation.^[9,10]

Emerging applications of cell spheroids are also found in tissue engineering as constructs for implantable materials and as building blocks in bioprinting of complex 3D structures.^[11] In all these applications, the mechanical behavior^[12] of cell spheroids, in concert with the biochemical cell machinery, plays a key role not only in physiological processes, such as development and regeneration, but also in disease,^[12] for

example, being a critical factor in cancer progression and metastasis.^[13–15]

Historically, the interest in cell spheroids stemmed from the study of morphogenesis thanks to the seminal work of Wilson,^[16] Holtfreter^[17] and other authors,^[18] which inspired Steinberg et al. in developing the differential adhesion hypothesis^[19] (later modified as the differential interfacial tension hypothesis^[20,21]), based on the analogy with phase separation of immiscible fluids, and the tissue surface tensiometer to measure the apparent tissue surface tension (ATST).^[22] In fact, both emulsions and cellular spheroids are characterized by attractive interactions, and the presence of an equivalent surface tension can be envisaged to explain the resistance of spheroids to deformation and coalescence.^[23]

In most of these works, cell spheroids are compressed in a parallel plate apparatus and the stress relaxation (annealing) data at times in the order of minutes are fit to theoretical models^[24,25] to extract the ATST and other mechanical parameters. The proposed picture is that, following an initial elastic deformation, cell rearrangement at longer times could be described in terms of the ATST.

Further experimental advances to characterize cell spheroids mechanical behavior, such as the Young's modulus and characteristic relaxation times, include other techniques, such as isotropic compression by osmotic pressure,^[26,27] atomic force microscopy (AFM),^[28,29] micro-indentation,^[30] tweezers,^[31] cavitation rheology^[32,33] and elastography.^[34,35] Each of these methods has its own strengths and limitations, and their results, in terms

R. Ferraro, S. Caserta, S. Guido

DICMaPI

Università degli Studi di Napoli Federico II
P.le V. Tecchio 80, Napoli 80125, Italy

E-mail: sergio.caserta@unina.it

R. Ferraro, S. Caserta, S. Guido

CEINGE-Biotecnologie Avanzate Franco Salvatore
Via Gaetano Salvatore, 486, Napoli 80131, Italy

 The ORCID identification number(s) for the author(s) of this article can be found under <https://doi.org/10.1002/admt.202301890>

© 2024 The Authors. Advanced Materials Technologies published by Wiley-VCH GmbH. This is an open access article under the terms of the Creative Commons Attribution-NonCommercial-NoDerivs License, which permits use and distribution in any medium, provided the original work is properly cited, the use is non-commercial and no modifications or adaptations are made.

DOI: [10.1002/admt.202301890](https://doi.org/10.1002/admt.202301890)

of Young's modulus, can vary, depending on the specific technique used, as shown in Table S1 (Supporting Information) for different immortalized cell lines and human biopsies.

Additionally, mechanical properties are also dependent on size^[36] and growth conditions of the cell spheroids,^[37] showing a time-dependent viscoelastic behavior, influenced by factors such as cell-cell adhesion and extracellular matrix production.

Although the aforementioned techniques have provided important scientific insights on the mechanical behavior of cell spheroids, they are based on specialized equipment and technical skills that are not usually available in cell biology facilities. Simple, more accessible experimental methods to measure the mechanical properties of cell spheroids are highly needed. Ideally, such methods should be compatible with standard cell culture techniques and rather inexpensive to allow the high-throughput scale that is often required when addressing biological problems. The need to test large number of samples to measure a few experimental parameters of simple interpretation in a standardized way is especially important in studying disease, where high variability is expected and tools allowing to correlate data are quite important.

Here, we propose an innovative rheo-optical compression assay based on simple materials and equipment usually available in a biology lab. Our approach is based on the combination of a constant stress test (creep) by using a microscope coverslip to apply the load and data fitting of the resulting deformation with rheological models^[36] to extract mechanical parameters. The assay is first validated on agarose gel particles and then carried out on two different cell lines to exemplify its application. Additionally, it offers a straightforward and economical alternative for measuring spatio-temporal biophysical changes in biological samples, addressing a significant current demand.^[38–44]

2. Results and Discussion

2.1. Analyzing Gel Particle Deformation with Rheo-Optical Compression Assay

Our main objective is to develop a methodology that allows us to perform a quantitative mechanical characterization of cell spheroids by using standard equipment easily available in cell culture facilities. Preliminary tests have been carried out on spherical particles made of agarose gel. The preparation of these particles is illustrated in Figure 1 and described in more detail in the Experimental Section (Preparation of Agarose Gel Particles). Briefly, a droplet of a hot 2.5% agarose solution in water is gelled by immersing it in silicone oil at room temperature. Two images of the so obtained agarose gel particle in the side and top view, the former taken by a smartphone with additional optics and the latter by a light microscope, are shown in Figure 1a (left), where the red color is due to the addition of Rhodamine B to the agarose solution. The agarose gel particle is then transferred into a cell culture plate filled with silicone oil. A microscope coverslip is placed on the agarose gel particle by using a 3D printed frame (see Figure 1b) as a positioning guide (see Video, Supporting Information). Under such a mechanical load, the agarose gel particle is compressed, as illustrated by the side and top view images (recorded once equilibrium has been reached), which are in-

cluded in Figure 1a (right) as well. The two images show that the agarose gel particle is deformed with respect to the initial spherical shape. The deformation can be described in terms of the distance R' between particle center and lateral surface with respect to the initial radius R (see Figure 1 (right)). Another measure of particle deformation is given by the vertical displacement d with respect to R (see Figure 1 (right)). By placing more coverslips, further compression is imposed, and the resulting deformation can be obtained by analysing the shape of the compressed agarose gel particle. For the sake of simplicity, only top view images are taken in the experiments (by light microscopy).

2.2. Elastic Modulus Measurement Validation via Gel Particle

The rheo-optical compression test previously described involves the progressive application of several coverslips, one at a time, on the agarose particle by means of the 3D printed guide shown in Figure 1b. Equilibrium conditions are allowed to be reached after each coverslip is added (that takes a few minutes, as shown in the next subsection). Figure 2a shows representative phase-contrast microscopy images of agarose particles compressed under different loads. From left to right the agarose particle is subject to stresses ranging from 0 to $3.02 \cdot 10^4$ Pa, with the latter corresponding to a load of five glass coverslips. The images show that both the contact area and the distance R' between the center and the lateral surface of the deformed agarose particle increase with the applied load. However, the increase in R' relative to R is relatively small. The penetration depth, δ , which is the vertical displacement of the coverslip, can be calculated by volume conservation. If the lateral profile of the deformed agarose particle is taken as a circular arc (as suggested by the side view of Figure 1a right), the penetration depth can be obtained from Equation (1)^[45]:

$$\frac{4}{3}\pi R^3 = 2\pi R'^2 (R - \delta) - \frac{2}{3}\pi(R - \delta)^3 \quad (1)$$

(a similar value is found by assuming an elliptical shape of the lateral profile, see Materials and Methods). From the so obtained value of δ , the vertical deformation ϵ can be calculated as δ/R .

The plot of the compression stress σ versus the deformation ϵ , shown in Figure 2b, reveals a linear correlation between these two quantities. By fitting the data to Hooke's law, a Young's modulus E of $8.4 \cdot 10^4$ Pa can be obtained.

To validate the Young's modulus obtained from the gel particle compression test, we compared it to values obtained using independent, well-established experimental methods. We employed two techniques based on a rotational rheometer with a parallel plate configuration: an unconfined compression testing (Figure 2c) and an oscillatory shear testing in the linear viscoelastic regime (Figure 2d). In the unconfined compression test, an agarose solution sample is loaded between the plates and let to gel at room temperature. The upper plate is then brought to a lower position and the compression force F_N is measured using the rheometer's normal force transducer. The compression stress σ is calculated as the measured force divided by the area of the plates, while the strain ϵ is obtained as the ratio of the current and initial values of the gap between the plates. The resulting stress-strain data, plotted in Figure 2c, exhibit a linear trend within the

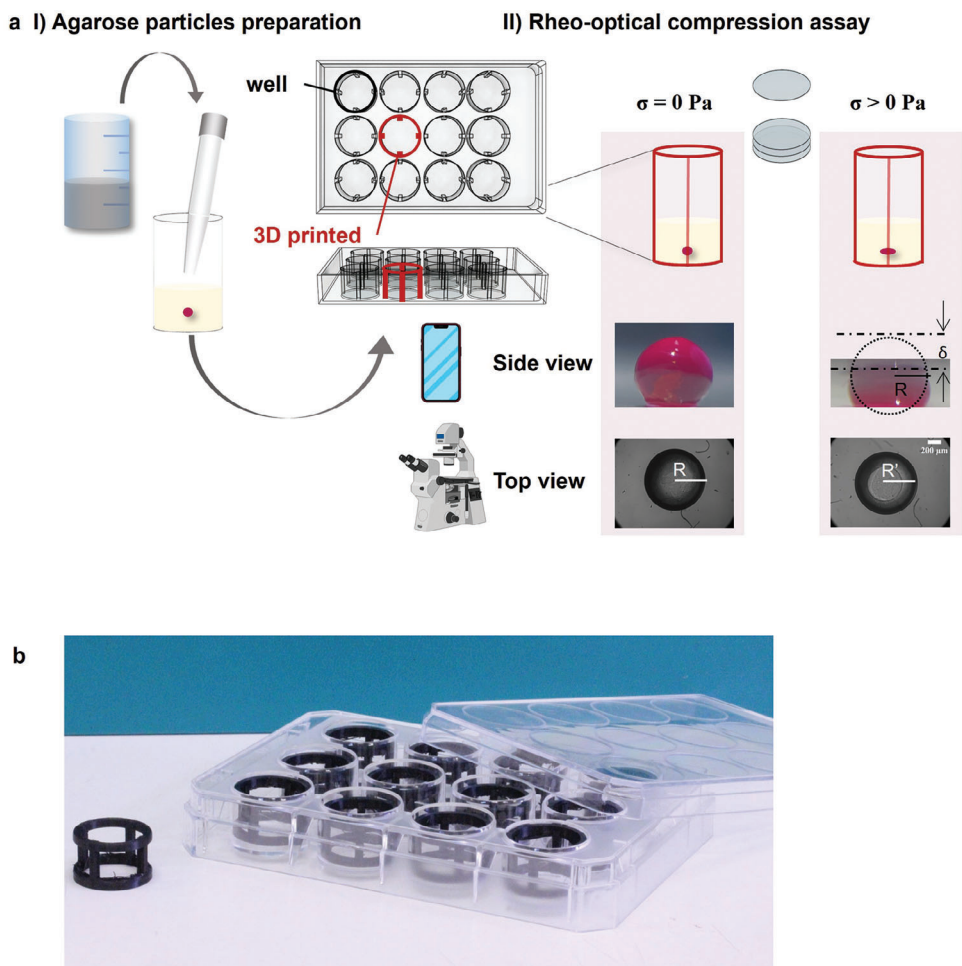


Figure 1. a) Preparation of agarose particles (refer to section 'Preparation of agarose gel particles' for detailed methodology) and our rheo-optical compression assay scheme. Morphological response of an agarose particle, taken as a qualitative representation of a given experimental condition, with an applied stress $\sigma > 0$ Pa (second column), recorded by means of smartphone (first row) and microscope (second row), compared to the control condition ($\sigma = 0$ Pa, first column). b) A custom-designed 3D printed guide for the coverslip used in the rheo-optical compression assay. The guide, shown in black, ensures precise placement and alignment during the assay process. See Video S2 (Supporting Information) for more detail.

investigated range. The slope of the linear fit provides a value of the Young modulus of $2.9 \cdot 10^5$ Pa, which aligns well with the value obtained from the compression test of the agarose gel particle; the slight discrepancy could be attributed to the influence of interfacial tension acting on the lateral surface of the gel between the plates.

In the oscillatory shear test, an agarose solution sample is allowed to gel between the parallel plates, as in the unconfined compression test. The upper plate is then subjected to an oscillatory motion at low amplitude to ensure that the sample is tested in the linear viscoelastic regime. The results of the test are given in terms of the elastic and viscous moduli, G' and G'' , respectively, as a function of the frequency ω , as shown in Figure 2d. As expected in the case of a solid-like gel material, G' consistently exceeds G'' , and the two moduli follow a nearly parallel trend across the entire frequency range investigated. Oscillatory shear measurements are performed both before (triangles up) and after (triangles down) the compression test of the agarose gel sample. No significant difference is observed between

the two sets of data for the loss modulus G'' (orange symbols). On the contrary, G' (gray symbols) exhibited a slight increase of $\approx 25\%$, indicating a mild compressional stress stiffening behavior, consistent with previous findings.^[46] In the linear viscoelastic regime, the elastic modulus E can be calculated from the shear modulus G from Equation $E = 2(1 + \nu) G$, where ν is the Poisson's ratio, assumed to be 0.5. By taking $G = \sqrt{G'^2 + G''^2} = 6.7 \cdot 10^4$ Pa from the data of Figure 2d, an estimate of $E = 2.0 \cdot 10^5$ Pa can be obtained, which again aligns well with the value of E obtained from the compression test of the agarose gel particle.

The compression assay on the gel particle demonstrates its effectiveness in determining the elastic modulus. This suggests that the same technique can be applied to cell spheroids, which are the focus of this study. As we move into the next section, which focuses on the compression test of cell spheroids, it is noteworthy that the agarose gel employed in this work exhibits a non-negligible viscous modulus, as shown in Figure 2d, although much smaller than the elastic one. The presence of a viscous

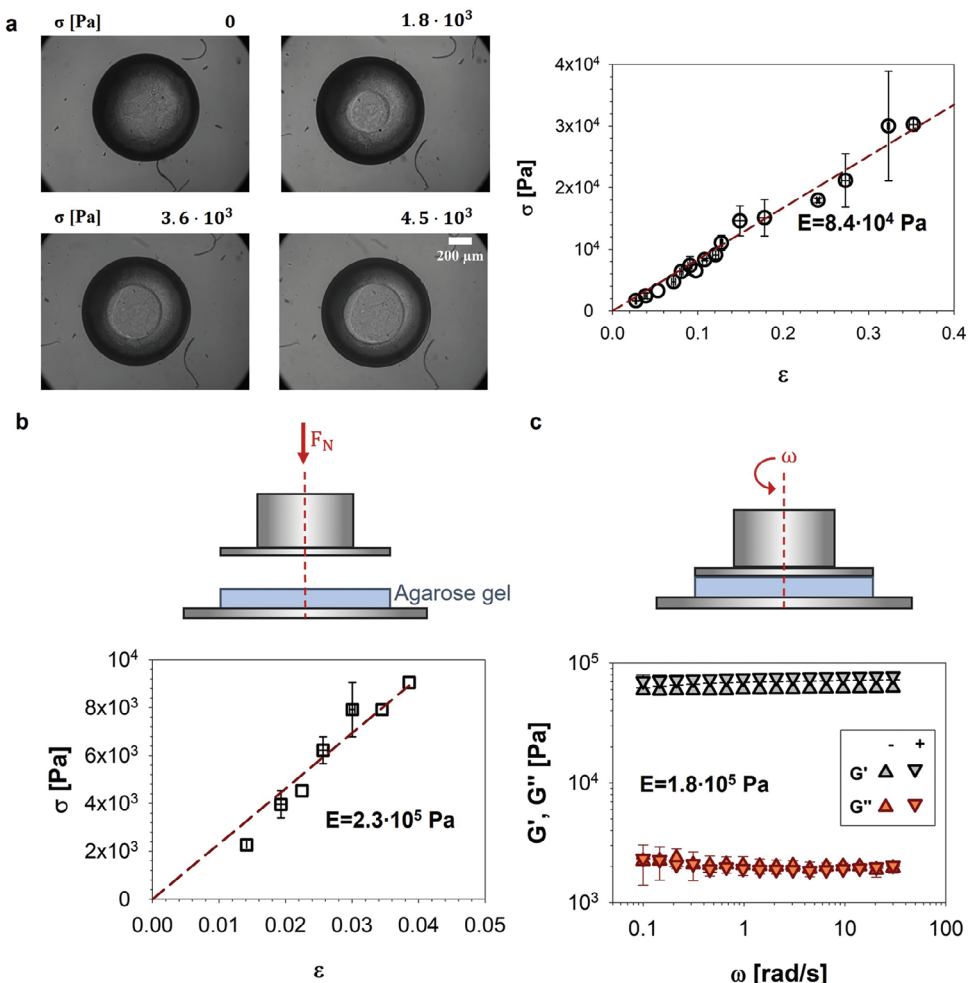


Figure 2. a) left) Representative phase-contrast microscopy images showing the morphological changes of agarose particles under different applied stress, σ , ranging from 0 to $\approx 5 \cdot 10^3$ Pa). The variation corresponds to an increasing number of coverslip glasses. Scale bar: 200 μm . a right) Stress–strain relationship from our rheo-optical compression assay. The data points are plotted with the applied stress, σ , versus the strain, ϵ , and the dashed line indicates a linear fit to the experimental data. b) Compression stress versus strain plot derived from tests using a rotational rheometer. The dashed line represents a linear fit. c) The shear storage modulus ($G'(\omega)$, represented by gray triangles) and the shear loss modulus ($G''(\omega)$, represented by orange triangles)) versus the angular frequency (ω), obtained by oscillatory tests, for agarose particles, before (upward-pointing triangles) and after (downward-pointing triangles) the compression test performed in the same rotational rheometer. All the data are calculated as average \pm standard deviation, over at least two independent measurements (overall 15 independent measures being available in the entire range investigated). The horizontal error bar is merely visible, being smaller than bullet size.

component in the rheological behavior can be linked to the transient response following the application of a mechanical load (see next subsection).

2.3. Probing Cell Spheroid Mechanics with Rheo-Optical Compression Assay

The cellular spheroids for the rheo-optical compression test are prepared according to the method described in 'Cell Culture and Spheroids Formation' section. As schematically shown in Figure 3a, the cell spheroids are transferred by using a pipette in a multiwell plate pre-filled with standard culture medium. The 3D printed insert is then used to immerse the coverslips in the cul-

ture medium, thus compressing the spheroid, and the multiwell plate is placed on the motorized stage of an inverted microscope. Top view microscopy images of a representative spheroid (made of NIH/3T3 cells) are shown with and without the applied stress ($\sigma = 0$ Pa and $\sigma > 0$ Pa) in the bottom of Figure 3b. It can be noticed that, at variance with the compressed agarose gel particles, the cell spheroids are quite flattened right after the application of the first coverslip, thus taking an essentially cylindrical shape. The same procedure can be applied to study the transient deformation of the cell spheroid following the application of a coverslip until a steady state is reached. In all the experiments the stress is calculated by dividing the weight of the applied coverslips (minus the Archimedean lift) by the area of the compressed cell spheroid.

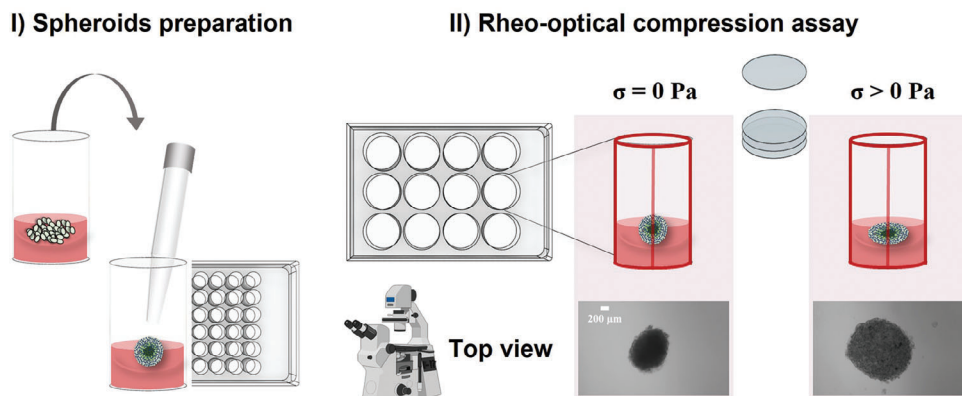


Figure 3. Methodology from cell aggregation to spheroid formation (detailed in section 'Cell culture and spheroids formation') and a schematic of the rheo-optical compression assay. The bottom images depict optical microscopy views of an NIH/3T3 spheroid, serving as a representative sample. It shows the spheroid's morphology before ($\sigma = 0 \text{ Pa}$) and after ($\sigma > 0 \text{ Pa}$) compression, which is achieved by applying glass coverslips.

2.4. Elastic Moduli Evaluation by Steady State Stress–Strain Outcomes

Representative phase-contrast microscopy images showing the morphological response of NIH/3T3 and PANC-1 spheroids at four different values of σ (from 0 to $\approx 4 \cdot 10^4 \text{ Pa}$), corresponding to an increasing number of coverslips as the applied load, are reported in Figure 4a,c, respectively. The images show that spheroids of both cell lines get progressively more deformed by increasing the applied load, the more so for the PANC-1 spheroids, which is likely related to their tumor phenotype. A quantitative representation of applied load versus measured deformation is given by the stress-strain data in Figure 4b,d, where data of a single representative spheroid are presented in the left plot and the average small deformation behavior of at least 15 spheroids are shown in the right plot. The single spheroid data (left plot) of both cell lines exhibit a linear trend up to a value $\epsilon^* \approx 1$ (region highlighted in yellow), followed by a sharp rise at larger deformations.

As done in the analysis of the agarose gel particles, we have averaged the data from different spheroids at $\epsilon < \epsilon^*$ and then fit a linear function to the so obtained results with the elastic modulus E as the only fitting parameter. The so calculated values of E are $(5.4 \pm 0.7) \cdot 10^4 \text{ Pa}$ for NIH/3T3 and $(1.9 \pm 0.3) \cdot 10^3 \text{ Pa}$ for PANC-1 spheroids. These values fall within the range of the elastic modulus of spheroids from different cell lines reported in the literature by using several techniques (see Table S1, Supporting Information). Although our experimental results are still quite preliminary and just meant to exemplify the application of the compression test developed in this work, it can be noticed that the value of E for the PANC-1 tumor cell line is much lower than the one for the NIH/3T3 cell line. This result is in line with the finding that tumor cell spheroids are generally softer than spheroids from healthy cell lines, such as tumor cells are apparently softer than their healthy counterparts.^[12] Other variables can also affect the mechanical properties of cell spheroids, such as the cultivation time, the spheroid size and the extent and composition of the extracellular matrix around the cells of a spheroid. We believe that a quantitative investigation of the effect of such variables is one of the main outcomes that can be obtained by a sys-

tematic application of the compression test here proposed. A detailed study of the mechanical behavior of cell spheroids as a function of the relevant variables is however outside the scope of this work.

2.5. Rheological Models for Cell Spheroids

Apart from the measurement of the elastic modulus in the linear regime, the compression test can also be used to evaluate the applicability of rheological models in describing the entire mechanical response of cell spheroids, including the large deformations region at $\epsilon > 1$. In this region, the rapid increase in stress with increasing strain resembles the mechanical behavior of polymeric foams under uniaxial compression.^[47] An analogy between foams and cell spheroids has been proposed in the literature^[48] based on the observation that both materials are characterized by packings of soft particles, bubbles in foams and cells in spheroids.

Among the rheological models available in literature,^[49] we have used, as an example, a phenomenological model originally developed to describe the mechanical behavior of foams.^[50] The model, schematized in Figure 5a, consists of three elements in a parallel combination: a linear spring with an elastic constant k_p , a linear spring with elastic constant k in series with a dashpot with viscosity c , and a nonlinear spring with deformation-dependent coefficient k_D . The linear spring and the series combination of spring and dashpot represent the elastic and viscous properties, respectively. The nonlinear spring is based on the so-called densification concept, which occurs when the cells in a foam become closely packed at high compressions. More details about the model parameter are provided in 'Phenomenological Model of Foam Compression' section.

As reported in Figure 4b,c, the experimental data (circle symbols) for cell spheroid deformation under a constant load are fitted using the following Equation:

$$\sigma = [k_p + \gamma(1 - e^\epsilon)^n \epsilon] \epsilon + \frac{c}{k} [k + k_p + \gamma(1 - e^\epsilon)^n \epsilon] \dot{\epsilon} \quad (2)$$

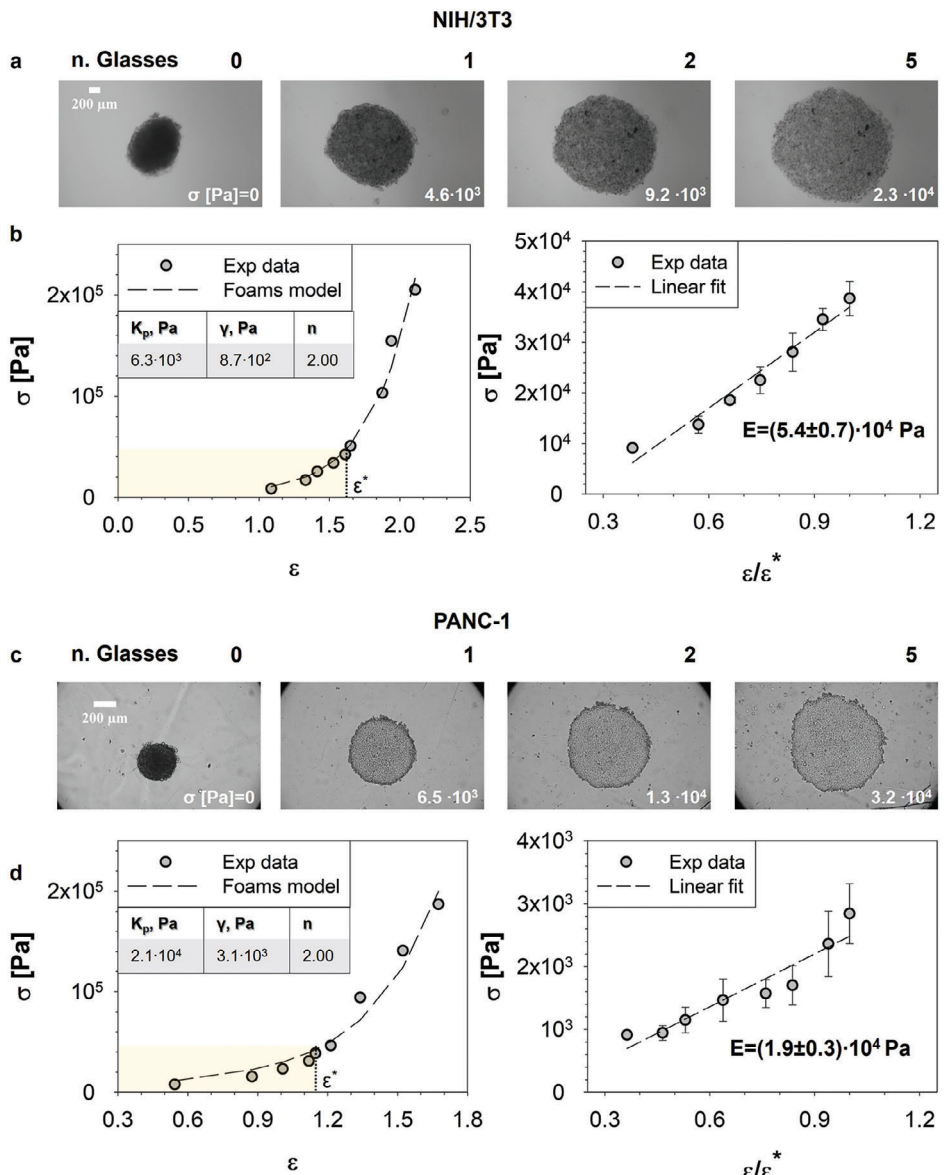


Figure 4. a,c) Representative phase-contrast microscopy images showing the morphological response of NIH/3T3 and PANC-1 spheroids under four different applied stress, σ , ranging from 0 to $\approx 4 \cdot 10^4$ Pa. This change in stress correlates with an increasing count of coverslip glasses used. Scale bar: 200 μ m. b,d, left) Stress–strain value quantified for a single representative spheroid of NIH/3T3 and PANC-1 cell line. The dashed curve is a fit of the foams model described in subsection 2.5. The yellow-highlighted area indicates the data range used to compute the Young's modulus up to the strain value (ϵ^*). (b,d, right) The Young's modulus, denoted as E , derived from the linear region of the stress–strain plot ($\epsilon < \epsilon^*$) for both NIH-3T3 and PANC-1 spheroids, respectively. The data points are the mean \pm standard deviation based on a minimum of two independent experiments, totaling 15 measurements across the investigated range.

derived from the Goga's phenomenological model^[50] (blue line). This model effectively describes not only the linear relationship between σ and ϵ , but also the densification (non-linear) region. Residual standard deviations (RSD) is $2.7 \cdot 10^4$ and $1.1 \cdot 10^3$, for NIH/3T3 and PANC-1, respectively. By fitting the data of 15 cell spheroids for each cell line, the values of the parameters k_p , γ and n shown in the table of Figure 5b are obtained.

The viscosity parameter c of the model is determined by analysing the transient behavior under compression. Images of

the cell spheroids are taken as a function of time after applying the coverslip load, until a steady deformation is reached. As an example of the observed experimental trends, the transient deformation is plotted in Figure 5 in the case of an NIH/3T3 spheroid (c) and a PANC-1 (d) spheroid. A plateau value is reached after ca. 100 s in the case of the NIH/3T3 spheroid, while for the PANC-1 spheroid a steep rise is followed by continuous growth at a slower slope. In any case, the observed time scale to reach a steady state (ca. 100 s) is well below the characteristic time for a significant cellular rearrangement within a spheroid. In the limit of

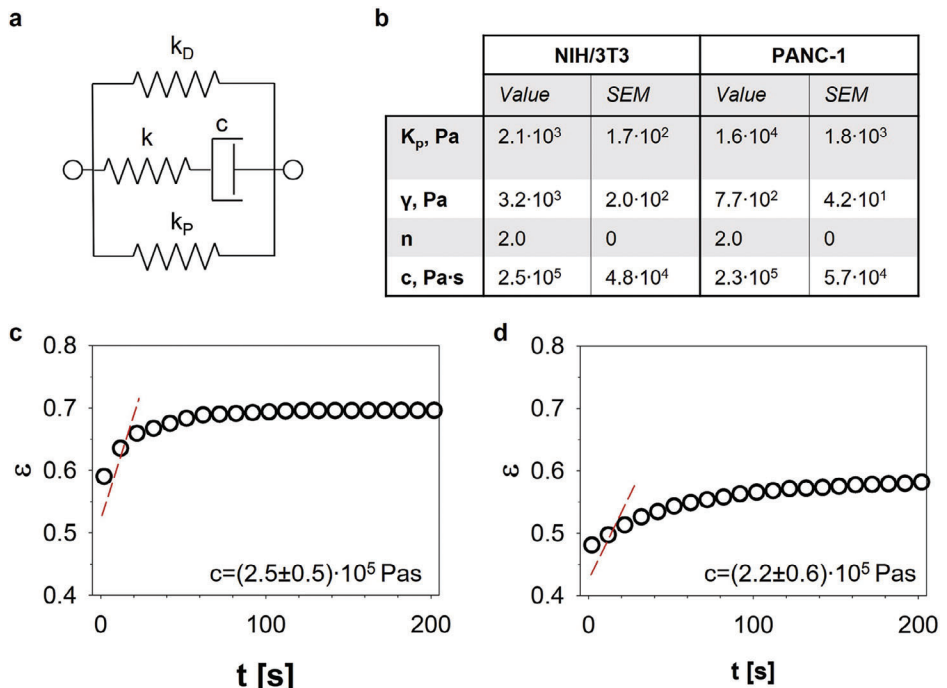


Figure 5. a) Diagram illustrating the phenomenological model used to interpret experimental data. The model components represent various mechanical properties within the system. b) The table lists the model parameters (steady-state: k_p , γ and n ; transient: c) derived from fitting the experimental data for NIH/3T3 and PANC-1 spheroids. c,d) Transient strain ϵ versus time for a NIH/3T3 and PANC-1 spheroid, respectively. The initial slope at $t = 0$, depicted by dashed lines, informs the computation of the transient parameter (c) as listed in the table in panel (b). Videos S3 and S4 (Supporting Information) demonstrate these dynamics.

vanishing deformation, the Goga's phenomenological model reduces to the Equation:

$$\sigma_{\epsilon \rightarrow 0} = \frac{c}{k} (k + k_p) \dot{\epsilon} \quad (3)$$

from which the initial slope can be obtained as:

$$\dot{\epsilon}(t = 0) = \frac{k \sigma}{c(k + k_p)} \quad (4)$$

By taking $k \gg k_p$, which is typical for the compression of foams, the initial slope can be approximated as:

$$\dot{\epsilon}(t = 0) \approx \frac{\sigma}{c} \quad (5)$$

The initial slope of the transient experimental data for a given applied stress can be used to calculate the viscosity parameter c , which is also included in Figure 5b and has essentially the same value for the two cell lines.

3. Conclusion

In this work, we introduce a pioneering rheo-optical compression assay that employs standard microscopy glass coverslips for load application in the mechanical characterization of cell spheroids. This technique, suitable for any biology laboratory with basic cell culture capabilities, simplifies the measurement

process. Cell spheroids, easily transferred to culture plate wells via pipette, are subjected to compression using coverslips strategically placed within 3D printed inserts. The compression can be visualized using standard laboratory equipment like an inverted microscope, or even a cell phone, capturing both transient and steady states. Simple image analysis techniques are then utilized to assess spheroid size and deformation, from which stress and deformation metrics are derived. Our assay's effectiveness is validated through application on an agarose gel particle, with its rheological parameters independently verified.

While the primary focus is on calculating the elastic modulus from the stress versus deformation curve's linear region, the assay's versatility extends to extracting other rheological parameters. This is achieved either by employing existing literature models or by innovating new ones. For instance, we have successfully applied a phenomenological model, originally designed for foam mechanics, to our dataset. This approach, effective in both transient and steady-state analyses, includes the crucial aspect of densification at high deformations, a process marking the compaction of the sample as foam cells undergo collapse. In cell spheroid studies, volume changes due to fluid loss occur at relatively large values of the imposed stress ($\approx 15\%$ at 15 kPa and 17% at 40 kPa for CT26 cells^[27]), likely due to water outflow from the extracellular matrix (ECM), which is estimated to take $\approx 15\%$ of the total volume. Therefore, in the linear range for calculating the elastic modulus, the volume of the cell spheroid can be assumed to remain essentially constant. Our employed phenomenological foam model adeptly accounts for the densification of cell spheroids at elevated deformations. While further

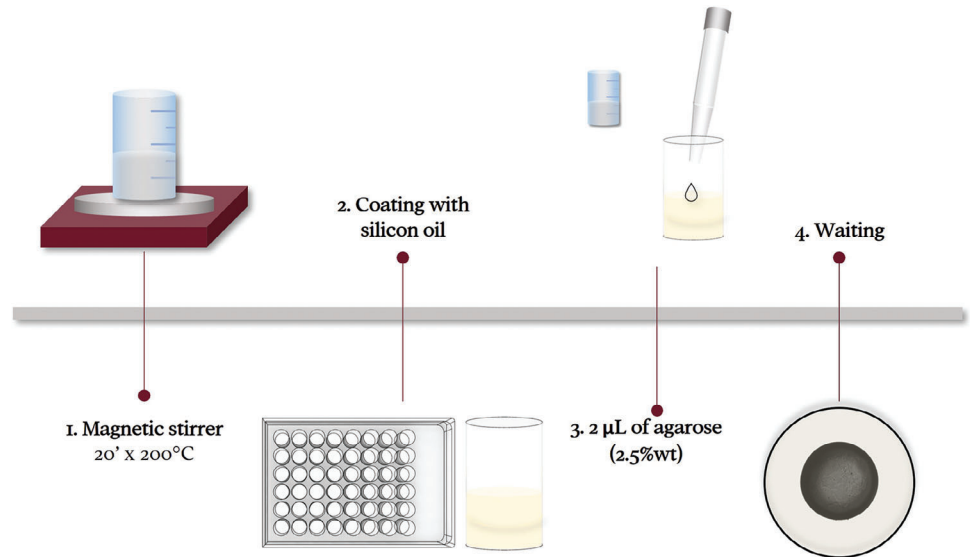


Figure 6. Step-by-step schematic of the agarose particle formation process. 1) Preparation of the aqueous agarose solution using a magnetic stirrer hotplate set at 200 °C for 20 min to ensure complete dissolution. 2) Pipetting of the hot agarose solution into a multi-well plate containing 600 μ L of low viscosity silicone oil for coating. 3) Dispensing 2 μ L of the agarose solution into the oil to initiate gelation and particle formation through rapid cooling. 4) A period of waiting, allowing for the solidification and stabilization of the formed agarose particles.

exploration in this domain is conceivable using our compression assay, such investigations fall outside the purview of our current study.

The integration of our compression assay into standard cell culture plates represents a significant innovation, notable not just for its widespread laboratory applicability but also for its compatibility with established biological methods for testing

diverse conditions. In contrast to other cell spheroid characterization techniques in the literature, which, while precise and sophisticated, often require specialized equipment and are not conducive to large-scale biological testing, our method stands out for its user-friendliness and versatility. Beyond cell spheroids, the assay is adaptable to samples like tissue biopsies, underscoring its broad potential impact in the field of mechanobiology.

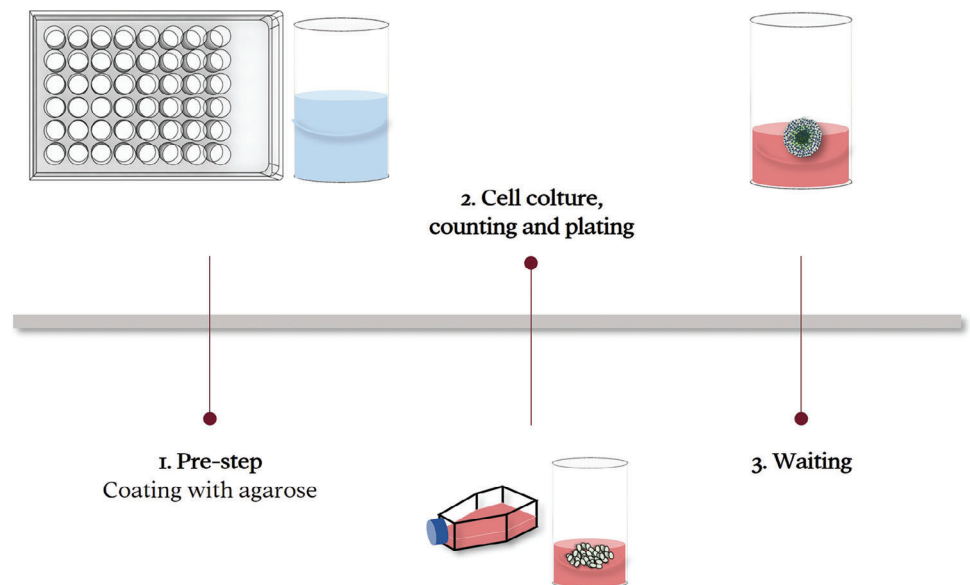


Figure 7. Overview of the spheroid formation procedure. The spheroid formation is delineated through the following sequential steps: 1) Preparation of Agarose Coating: A 2% (wt./vol) agarose solution is swiftly pipetted in 200 μ L aliquots into the wells of a 48-well culture plate. The solution is left to cool, leading to gelation and the formation of a hemispherical meniscus within each well. 2) Cell Seeding: Cells, after being cultured in a standard 2D monolayer and counted, are transferred into the agarose-pre-coated wells. These wells are then filled with the appropriate growth medium to support cell proliferation and spheroid development. 3) Spheroid Maturation: Over a period of 5–10 days, depending on the specific cell line, cells aggregate to form compact spheroids within the non-adhesive agarose environment.

research. However, further work is still required to provide systematic and extended validation of the technique, in particular comparing it with already established and widely used techniques, such as AFM. The mechanical properties of spheroids, as determined by our assay and compared with existing literature in the Table S1 (Supporting Information), could be pivotal in cancer diagnosis and prognosis.^[51] This underscores the assay's potential as a significant tool in the ongoing advancement of cancer research, particularly in the nuanced understanding and application of mechanical biomarkers.

4. Experimental Section

Preparation of Agarose Gel Particles: A 2.5% wt. aqueous solutions of agarose (Agarose E, Condalab, #8100) was prepared on a hot plate magnetic stirrer at 200 °C for 20 min. Rhodamine B (Rhodamine B (C.I.45170) for microscopy 81-88-9) was added to the agarose solution enhance of image clarity. As shown in Figure 6, 2 μL aliquots of aqueous solutions of agarose were rapidly transferred by a pipette into a cell culture multi-well plate (Nunclon Δ Multidishes, 48 wells, flat bottom, Thermo Scientific, Nunc 150 687) filled with 600 μL low viscosity silicone oil (Silicone oil 20 cSt 25 °C, 63148-62-9, Sigma-Aldrich) at room temperature. The abrupt cooling of the agarose solutions induces gelation, forming spherical particles suspended in the oil phase. The resulting spherical gel particle was aspirated with a pipette and transferred to a 35 mm Petri dish filled with silicone oil, non-miscible with respect to the water agarose solution.

The load was applied by gently immersing a microscope coverslip (24 mm × 24 mm, thickness 0.13–0.16 mm, weight 0.21 g, Knittel glass n. VD12424Y1A.01) in the silicone oil, ensuring it is centered with respect to the agarose gel particle. This procedure can be facilitated by drawing a center target, marked as the intersection of the two diagonals of the square coverslip, using a glass marker and a ruler. Additionally, sedimentation of the glass respect to the agarose particle was regulated by hydrodynamic of viscous medium that resulted in symmetric friction forces due to the partial confinement respect to the Petri dish. Once glass coverslip compresses the sample, flow stops, and no further viscous stresses were present.

Cell Culture and Spheroids Formation: One cancer cell line (PANC-1) and a non-tumor one (NIH/3T3) were used. All cells were cultured in their standard growth medium in 2D monolayers under the typical cell culture conditions, at 37 °C in a humidified atmosphere (5% CO₂). NIH/3T3 mouse fibroblasts and PANC-1 human pancreatic carcinoma cells were cultured in Dulbecco's Modified Eagle's Medium (DMEM) supplemented with 10% (v/v) Fetal Bovine Serum (FBS), 1% (v/v) antibiotics (50 units/mL penicillin and 50 mg mL⁻¹ streptomycin) and 1% (v/v) L-glutamine.

Spheroids were produced using the liquid overlay technique.^[7,23] Specifically, a 1% agarose solution was prepared by dissolving agarose powder (E AGAROSE, Conda, Cat n° 8100) in water at 200 °C for 20', using a magnetic stirrer to homogenize the solution. The agarose solution was then rapidly pipetted in 200 μL aliquots into the wells of a 48-well culture dish (Nunclon Δ Multidishes, 48 wells, flat bottom, Thermo Scientific), as shown in Figure 7, under sterile conditions. The agarose solution cools down and, by capillarity, rises along the walls of the wells, thus gelifying in a few minutes and forming a hemi-spherical meniscus. The non-adhesive concave surface promotes the collection of cells in the meniscus and cell-cell adhesion establishment. This results in the formation of cell aggregates and finally spheroids after an adequate incubation time, depending on cell type and concentration.

To generate spheroids, cells were harvested from monolayer cultures and counted. 8 • 10³ and 3 • 10³ NIH/3T3 and PANC-1 cells, respectively, were seeded in single wells pre-coated with non-adhesive agarose and covered with the cell growth medium. The multiwell plate was then incubated under typical cell culture conditions at 37 °C to allow spheroid formation. Typically, 5–10 days (depending on cell line) are required to obtain compact spheroids of adequate size. Minimum information of spheroids^[52]

for each cell lines are reported in Tables S2, S3 (Supporting Information) (NIH/3T3 and PANC-1, respectively).

Compression Test and Microscopy: The compression test involved placing one or more microscope coverslips onto a gel particle or cell spheroid. To aid in the positioning of the coverslips, a plastic frame was used as a guide, as shown in Figure 1b. This frame was designed using Autodesk Fusion 360 and printed in PVA material using Ender 3 S1 3D printer.

Spherical gel particles and spheroids morphological changes, as a function of stress applied, were observed by Laser Scanning Confocal Microscope (LSM) 5 Pascal (Carl Zeiss Advanced Imaging Microscopy, Jena, Germany). Several independent fields of view were acquired by a high-resolution high-sensitivity monochromatic CCD video camera (Hamamatsu Orca AG, Japan) using a 5 × and 10× objectives.

Image Analysis: In order to quantify mechanical stimuli effect on spheroids evolution, the morphological response of cellular spheroids, in terms of area and diameter (A and D, respectively), were measured by using an image analysis software (Image Pro Plus 6.0, Media Cybernetics). The measurement was taken on the diametral plane for each acquired image.

The evaluation of the area is crucial to quantify the applied stress. In details, the stress, σ , is defined as $(F_w - F_A)/A$, where F_w is the glass coverslips weight, while F_A is the Archimedes force, related to PBS in which spheroid is seeded. The applied stress, σ , is related to the local deformation, that is, the strain, referred as ϵ . To define ϵ as function of a measured parameter, the assumption of constant volume, before and after the compression, was made. In this way, the strain was evaluated as $\epsilon = \delta/R$, i.e., as the normalized penetration, δ , under compression.

Rheological Setup: Rheological measurements were performed by means of a stress controlled rheometer (Anton Paar Physica MCR 301 Instruments) equipped with parallel plates having diameters of 75 mm (PP75/T1/S-SN2005). Rheological tests were run at room temperature (23 °C), temperature was controlled by a Peltier cooler/heater connected to a circulating water bath (Lauda) and let to equilibrate at the measuring value for 3 min before each test.

In order to polymerize the sample between plates, rheometer temperature was set to 70 °C. Then ≈10 mL of agarose solution was distributed on the bottom plate, and the upper plate lowered to a gap of 2 mm. To limit water evaporation, ≈400 μL of oil (Wacker Wacker AK 5 Silicone Fluid) were added on sample edge. Pre-shear was run to homogenize sample structure after loading, imposing a constant shear rate ($\dot{\gamma}$) of 200 s⁻¹ for 1 min. Sample was cooled down to 23 °C and let to complete polymerization for 30 min before running rheological characterization.

Strain sweep experiments were performed to identify the linear viscoelasticity range. Storage and loss moduli (G' and G'' , respectively) were measured at two fixed angular frequencies ($\omega = 10$ and 1 rad s⁻¹) varying the strain in the range 0.01–10% and showed a linear behavior for strains lower than ≈0.5%. Frequency sweep was investigated at strain 0.05% varying frequency in the range 30–0.1 rad s⁻¹.

Rheo-optical compression test was reproduced also under the rheometer by imposing a step-by-step incremental compression of the sample between the two plates by applying controlled values of normal force (F_N), in the range 10–40 N, with steps of 5 N. For each value, F_N was kept constant for 10 min, while monitoring the value of sample gap (h). The compression stress applied is calculated as $\sigma = 4F_N/\pi D^2$, where D is the tool diameter, and related to the corresponding strain, calculated as $\epsilon = (h_0 - h)/h_0$, where h_0 is the initial value of gap (2 mm) and h is the current value of the gap, measured during the test.

Phenomenological Model of Foam Compression: The phenomenological model used to fit the compression data was the one proposed by Goga.^[50] As shown in Figure 5a, the model was based on the parallel combination of three elements: a linear spring with an elastic constant k_p , a linear spring with elastic constant k in series with a dashpot with viscosity c , and a nonlinear spring with deformation-dependent coefficient k_D . The Equations describing the mechanical behavior of the three elements are as follows:

$$\sigma_M = \sigma_K = \sigma_C \quad (6)$$

$$\epsilon_M = \epsilon_K + \epsilon_C \quad (7)$$

$$\sigma = \sigma_M + \sigma_P + \sigma_D \quad (8)$$

$$\varepsilon = \varepsilon_M = \varepsilon_P = \varepsilon_D \quad (9)$$

$$\sigma_K = k\varepsilon_K \quad (10)$$

$$\sigma_C = c\varepsilon_C \quad (11)$$

$$\sigma_P = k_p \varepsilon_P \quad (12)$$

$$\sigma_D = k_D \varepsilon_D = \gamma(1 - e^{\varepsilon_D})^{n\epsilon} \quad (13)$$

$$\dot{\varepsilon} = \dot{\varepsilon}_M = \dot{\varepsilon}_K + \dot{\varepsilon}_C = \frac{\dot{\sigma}_M}{k} + \frac{\dot{\sigma}_M}{c} \quad (14)$$

$$\sigma + \frac{c}{k} \dot{\sigma} = (k_p + k_D) \varepsilon + \frac{c}{k} (k + k_p + k_D) \dot{\varepsilon} \quad (15)$$

which then leads to Equation (2) in the constant stress case investigated in this work.

Statistical Analysis: Data in this study are presented as mean \pm standard error of mean (SEM). The SEM is a statistical tool that quantifies the amount of variability one might expect in a sample mean relative to the population mean, thereby facilitating statistical inference from the sampling distribution.^[53] It is calculated by dividing the standard deviation by the square root of the sample size.

For our rheo-optical compression tests, a minimum of 15 spheroids were analyzed for each cell line, encompassing both tumoral and non-tumoral types.

Supporting Information

Supporting Information is available from the Wiley Online Library or from the author.

Acknowledgements

Vincenzo Pepe contributed to the experiments, data analysis, and data interpretation as part of the master thesis. The authors would like to express the gratitude to Dr. Speranza Esposito and Dr. Valeria Rachela Villella for their invaluable support to cell cultures.

Conflict of Interest

The authors declare no conflict of interest.

Author Contributions

R.F. cultured cells, prepared spheroids, and agarose particles, performed rheo-optical compression tests and rheological measurement, performed all live imaging experiments, analyzed data and wrote the manuscript draft. S.C. and S.G. designed and supervised the project, provided funds, wrote, reviewed, and edited the manuscript. All authors approved the manuscript.

Data Availability Statement

The data that support the findings of this study are available from the corresponding author upon reasonable request.

Keywords

3D biology models, cell spheroids, mechanical characterization, rheological mode, rheo-optical compression assay, tumor stiffness

Received: November 17, 2023

Published online: January 4, 2024

- [1] X. Cui, Y. Hartanto, H. Zhang, *J. Royal Soc. Interface* **2017**, *14*, 20160877.
- [2] R.-Z. Lin, H.-Y. Chang, *Biotechnol. J. Healthcare Nutrit. Technol.* **2008**, *3*, 1172.
- [3] J. Carlsson, T. Nederman, *Europ. J. Cancer Clin. Oncol.* **1989**, *25*, 1127.
- [4] A. Nyga, U. Cheema, M. Loizidou, *J. Cell Commun. Signal.* **2011**, *5*, 239.
- [5] K M. Yamada, E. Cukierman, *Cell* **2007**, *130*, 601.
- [6] J. Hoarau-Véchot, A. Rafii, C. Touboul, J. Pasquier, *Intern. J. Mol. Sci.* **2018**, *19*, 181.
- [7] R. Ferraro, F. Ascione, P. Dogra, V. Cristini, S. Guido, S. Caserta, *AIChE J.* **2022**, *68*, e17658.
- [8] C K. N. Li, *Cancer* **1982**, *50*, 2066.
- [9] M. Dolega, G. Zurlo, M. Le Goff, M. Greda, C. Verdier, J.-F. Joanny, G. Cappello, P. Recho, *J. Mechan. Phys. Solids* **2021**, *147*, 104205.
- [10] V. Cristini, H. B. Frieboes, R. Gatenby, S. Caserta, M. Ferrari, J. Sinek, *Clin. Cancer Res.* **2005**, *11*, 6772.
- [11] A C. Daly, M D. Davidson, J A. Burdick, *Nat. Commun.* **2021**, *12*, 753.
- [12] Y M. Efremov, I M. Zurina, V S. Presniakova, N V. Kosheleva, D V. Butnaru, A A. Svistunov, Y A. Rochev, P S. Timashev, *Biophys. Rev.* **2021**, *13*, 541.
- [13] P. Gassmann, J. Haier, *Clin. Experim. Metastasis* **2008**, *25*, 171.
- [14] A. B. Mariotto, R. Etzioni, M. Hurlbert, L. Penberthy, M. Mayer, *Cancer Epidemiol., Biomarkers Prev.* **2017**, *26*, 809.
- [15] Q. T. Ostrom, C. H. Wright, J. S. Barnholtz-Sloan, *Handb. Clin. Neurol.* **2018**, *149*, 27.
- [16] H. V. Wilson, *J. Elisha Mitchell Sci. Soc.* **1907**, *23*, 161.
- [17] P L. Townes, J. Holtfreter, *J. Experim. Zool.* **1955**, *128*, 53.
- [18] J H. Shawky, L A. Davidson, *Developm. Biol.* **2015**, *401*, 152.
- [19] M S. Steinberg, *Science* **1963**, *141*, 401.
- [20] A K. Harris, *J. Theor. Biol.* **1976**, *61*, 267.
- [21] G. W Brodland, *J. Biomech. Eng.* **2002**, *124*, 188.
- [22] R A. Foty, G. Forgacs, C M. Pfleger, M S. Steinberg, *Phys. Review Lett.* **1994**, *72*, 2298.
- [23] D. Gonzalez-Rodriguez, K. Guevorkian, S. Douezan, F. Brochard-Wyart, *Science* **2012**, *338*, 910.
- [24] X. Shi, S. Jiang, L. Yang, M. Tang, D. Xiao, *Intern. J. Rock Mechan. Mining Sci.* **2020**, *127*, 104210.
- [25] E. Tanimoto, *Plant and Soil* **2000**, *226*, 21.
- [26] M. E. Dolega, M. Delarue, F. Ingremoine, J. Prost, A. Delon, G. Cappello, *Nat. Commun.* **2017**, *8*, 1.
- [27] M. E. Dolega, S. Monnier, B. Brunel, J.-F. Joanny, P. Recho, G. Cappello, *Elife* **2021**, *10*, e63258.
- [28] A. Ernad, W. F. Heinz, M. D. Antonik, D'N. P. Costa, S. Nageswaran, C.-A. Schoenenberger, J. H. Hoh, *Biophys. J.* **1998**, *74*, 1564.
- [29] A. Giannetti, J. Revilloud, C. Verdier, *Comp. Methods Biomed. Biomed. Eng.* **2020**, *23*, S125.
- [30] D. Jaiswal, N. Cowley, Z. Bian, G. Zheng, K P. Claffey, K. Hoshino, *Plos One* **2017**, *12*, e0188346.
- [31] S. Alhudaihy, K. Hoshino, *Plos one* **2022**, *17*, e0262950.
- [32] R C. Boot, G H. Koenderink, P E. Boukany, *Adv. Phys.-X* **2021**, *6*, 1978316.
- [33] S. Lee, K. M. I. Bashir, D. H. Jung, S. K. Basu, G. Seo, M-Gi Cho, A. Wierschem, *Interface Focus* **2022**, *12*, 20220036.
- [34] C.-E. Leroux, J. Palmier, A. C. Boccara, G. Cappello, S. Monnier, *New J. Phys.* **2015**, *17*, 073035.
- [35] D. Jaiswal, Z. Moscato, Y. Tomizawa, K P. Claffey, K. Hoshino, *Biomed. Opt. Express* **2019**, *10*, 2409.
- [36] A. Erlich, J. Étienne, J. Fouchard, T. Wyatt, *Interface Focus* **2022**, *12*, 20220038.
- [37] L. Guillaume, L. Rigal, J. Fehrenbach, C. Severac, B. Ducommun, V. Lobjois, *Sci. Rep.* **2019**, *9*, 1.
- [38] A. Blumlein, N. Williams, J J. Mcmanus, *Sci. Rep.* **2017**, *7*, 10.

- [39] D. Wang, H. G. Nguyen, M. Nakayama, H. Oshima, L. Sun, M. Oshima, S. Watanabe, *Small* **2023**, *19*, 2206213.
- [40] P. Saglam-Metiner, U. Devamoglu, Y. Filiz, S. Akbari, G. Beceren, B. Goker, B. Yaldiz, S. Yanasik, C. Biray Avci, E. Erdal, O. Yesil-Celiktas, *Commun. Biol.* **2023**, *6*, 173.
- [41] A. Karolak, D. A. Markov, L. J. Mccawley, K. A. Rejniak, *J. Royal Soc. Interface* **2018**, *15*, 20170703.
- [42] A. Ahmed-Cox, E. Pandzic, S. T. Johnston, C. Heu, J. Mcghee, F. M. Mansfeld, E. J. Crampin, T. P. Davis, R. M. Whan, M. Kavallaris, *J. Controlled Release* **2022**, *341*, 661.
- [43] L. Pulze, T. Congiu, T. A. L. Brevini, A. Grimaldi, G. Tettamanti, P. D'antonio, N. Baranzini, F. Acquati, F. Ferraro, M. De Eguileor, *Intern. J. Mol. Sci.* **2020**, *21*, 5400.
- [44] R. Knitsch, M. Alwahsh, H. Raschke, J. Lambert, R. Hergenröder, *Analyt. Chem.* **2021**, *93*, 13485.
- [45] Yu-Li Lin, Da-M Wang, W.-M. Lu, Yu-S Lin, K.-L. Tung, *Chem. Eng. Sci.* **2008**, *63*, 195.
- [46] R. Ferraro, S. Guido, S. Caserta, M. Tassieri, *Soft Matter* **2023**, *19*, 2053.
- [47] M. F. Alzoubi, S. Al-Hallaj, M. Abu-Ayyad, *J. Solid Mechan.* **2014**, *6*, 82.
- [48] D. L. Hu, S. Phonekeo, E. Altshuler, F. Brochard-Wyart, *The Eur. Phys. J. Special Topics* **2016**, *225*, 629.
- [49] G. Luo, Y. Zhu, R. Zhang, P. Cao, Q. Liu, J. Zhang, Y. Sun, H. Yuan, W. Guo, Q. Shen, *Polymers* **2021**, *13*, 3283.
- [50] *Computational Modelling and Advanced Simulations*, (Eds: M. Justín, V. Kompiš, V. Kutiš), Vol. 24, Springer Science & Business Media, **2010**.
- [51] V. Mihailef, R. I. Ionasec, P. Sharma, B. Georgescu, I. Voigt, M. Suehling, D. Comaniciu, *Interface Focus* **2011**, *1*, 286.
- [52] A. Peirsman, E. Blondeel, T. Ahmed, J. Anckaert, D. Audenaert, T. Boterberg, K. Buzas, N. Carragher, G. Castellani, F. Castro, V. Dangles-Marie, J. Dawson, P. De Tullio, E. De Vlieghere, S. Dedeyne, H. Depypere, A. Diosdi, R. I. Dmitriev, H. Dolznig, S. Fischer, C. Gespach, V. Goossens, J. Heino, A. Hendrix, P. Horvath, L. A. Kunz-Schughart, S. Maes, C. Mangoldt, P. Mestdagh, S. Michlíková, et al., *Nat. Methods* **2021**, *18*, 1294.
- [53] D. K. Lee, J. In, S. Lee, *Korean J. Anesthesiol.* **2015**, *68*, 220.